REMOTE IDENTIFICATION OF OPTICAL SYSTEMS BY TIME-GATED MULTI-WAVELENGTH RETRO-REFLECTION

Michel Auclair [1], Jean Fortin [2], Yunlong Sheng [1]

[1] Center for Optics, Photonics and Lasers, Laval University, Québec, Canada, G1K 7P4, Michel.Auclair.UN-LAVAL@drdc-rddc.gc.ca, sheng@phy.ulaval
[2] Defence R&D Canada - Valcartier, 2459 Boul. Pie XI N, Québec, Canada G3J 1X5, Jean.Fortin@drdc-rddc.gc.ca

ABSTRACT

We propose and demonstrate a multi-wavelength approach based on time-gated retro-reflection to discriminate false alarms from optical systems (OSs). Any objects other than optical systems are considered as false alarms. The detecting platform consists in a combination of a pulsed laser synchronized with a gated camera and a laser rangefinder. A Schmidt-Cassegrain telescope was modified to inject the light of laser sources and to collect the retro-reflected signal in a monostatic configuration.

The filtering method is based on the chromatic aberrations of the optical systems of interest which are measured using multiple interrogation wavelengths. A formula to evaluate the optical cross section (OCS) at the selected wavelengths is used for identification and relies on the system signature to discriminate the false alarms. We also explore the possibility to perform multiple simultaneous detections and target identification.

1. INTRODUCTION

Detection of optical systems is a real challenge as they are difficult to recognize in a complex background. Some studies have already shown the possibility to detect optical systems by using the technique of retro-reflection [1][2]. However, a robust solution has not yet been found to solve the problem of recognizing optical systems by retro-reflection in urban environment. In fact, retro-reflected signals of OS are often confused with spurious detections of many other objects that can reflect light.

In this article, an approach to discriminate false alarms from OS using a time-gated retro-reflection is first proposed. Then, the design of a platform for detection is presented and finally an experiment shows results that make possible to identify OS and discriminate false alarms.

2. APPROACH FOR IDENTIFICATION OF OPTICAL SYSTEMS

The term OS in this paper represents "any optical instrument which includes a focusing lens and a surface having some degree of reflectivity, no matter how small, positioned near the focal point of the lens" [2]. A retro-reflector is defined as "a reflector wherein incident rays or radiant energy and reflected rays are parallel for any angle of incidence within the field of view" [2]. An OS can act as a retro-reflector.

To be able to identify different OSs, it is necessary to associate them to their signature. As we are detecting radiation from retro-reflection, the signature must be calculated from the measured OCS.

In retro-reflection, the OCS [3] can be expressed as:

$$\sigma = \frac{\rho A}{\Omega} \qquad (1)$$

where ρ is the reflectivity, A the area of the target and Ω the solid angle of the return beam. By this definition, each OS has a different OCS. However, two systems can have very close OCS values and as it is calculated from detected radiation, it is possible to wrongly associate a value of OCS to objects that reflect light with a similar way than the retro-reflected signals of a target OS, hence causing false-alarms. One way to solve this problem is to use multiple laser sources with different wavelengths and measure the variation of the OCS as a function of the wavelength. As it is shown in the Fig. 1, the focalization point of rays, made by a set of lens inside an OS, may slightly be different depending on the wavelength of illumination. This phenomenon is caused by the variation of the refractive index of the lenses with the wavelength and also because the optical design is not always perfectly achromatic. To have a significant difference on the focalization point, it is important to use wavelengths with distant values, such as one in the visible and another one

in the near infrared. In fact, OS that are designed to be used in the visible are generally not achromatic in the near infrared region.

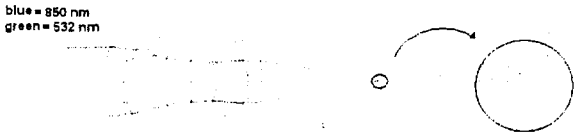

Figure 1. Illustration of the quality of focalization when using two different wavelengths (850 nm shown in blue and 532 nm in green) in a typical camera objective.

Optical simulations have been made on typical OSs to look at the impact of the wavelength on the focalization point. As shown in Fig. 2, the solid angle of the retro-reflected beam changes as a function of the illumination wavelength and at some distance the difference on the diameter is significant.

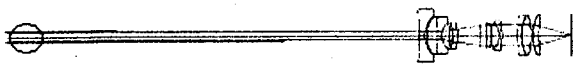

Figure 2. Illustration of diameter of the retro-reflected beam at 500 meters for an illumination sources at 532 nm (in green) and 850 nm (in blue).

Because all OSs have their own design, the variation between the OCS taken at different wavelengths is unique. This is useful to eliminate false alarms.

False alarms are defined as any objects other than OSs. For them, the variation in the OCS measured as a function of the wavelength is not in the same order. For example, a white retro-reflector installed on a car (or bicycle) has in theory an OCS independent of the wavelength because it is made of many small reflective mirror cavities that reflect light regardless of wavelength. The same phenomenon occurs for specular reflections on reflective materials.

3. DETECTION PLATFORM

The detection platform consists in a combination of a pulsed laser synchronized with a gated camera and a laser rangefinder. A Schmidt-Cassegrain telescope was modified to inject the light of laser sources and collect the retro-reflected signal in a monostatic configuration. Fig. 3 illustrates a preliminary version of a laboratory prototype.

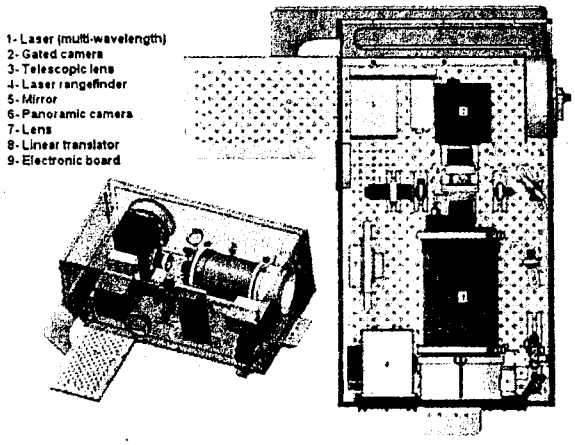

Figure 3. Platform designed for detecting retro-reflected signals.

The laser rangefinder gives the distance of objects in the area of interrogation. Then, a time-gated camera in synchronization with the pulsed laser produces a high contrast image of the signal retro-reflected by a potential target OS. The signal to noise ratio is increased by using interferential filters in front of the gated camera and centered on the wavelength of the laser source. Finally, the focus for getting the well-defined image at different distances is made by a translation of the gated-camera on a linear translator. The narrow field of view of the gated camera is centered in the field of view of a panoramic camera operating in the visible spectrum. This sensor gives a contextual view of the scene and helps the operator searching for areas of interest. Fig. 4 shows an image of the platform user interface. The top part shows an image produced by a panoramic camera. The bottom part shows the high contrast image of a 15 mm diameter retro-reflector at 600 meters in bright daylight.

Figure 4. View of the user interface.

The gated camera contains an imaging photocathode which converts photons to electrons. The photoelectrons are then accelerated by an electric field and multiplied by a micro channel plate. It consists of an array of millions capillaries

in a thin glass plate. Both faces of the plate are coated with thin metal films that act as electrodes and a voltage is applied across them. The interior walls of each capillary are coated with a secondary-electron-emissive material and behave as a continuous dynode, multiplying the photoelectron current emitted at that position. The local photon flux in an image can be rapidly converted into a substantial electron flux [4]. The highly intensified electron flux strikes a phosphor screen and provides electroluminescence that created an amplified image. Finally the image can be seen with a Silicon CCD camera which has horizontally 639 effective pixels and vertically 479 effective pixels. Each pixel has a dimension of 9.9μm x 9.9μm. The sensitivity of the photocathode is approximately 65 mA/W at a wavelength of 532 nm and 50 mA/W at 859 nm. The gain for amplification can be adjusted from 0 to 2500 mV.

4. THEORY OF THE EXPERIMENT

The purpose of the experimentation is to get data that will lead to a relation between retro-reflected signals and the OCS. The relation should be expressed by a mathematical formula. We first consider the theoretical relation between detected power in retro-reflection and the OCS [3]:

$$\Phi_R = \frac{\pi \Phi_T D^2}{4 \Omega_T R^4} \tau_1 \tau_2 \tau_T \tau_r \sigma \qquad (2)$$

where Φ_T is the transmitted power (W), Ω_T the transmitted-beam solid-angle (sr), τ_1 and τ_2 the one way path transmission, R the one-way range (m), D the receiver diameter (m), τ_T the transmitter optical transmission, τ_r the receiver optical transmission and σ the OCS of the target (m^2/sr).

Considering, one method to calculate the value of OCS is to measure the amount of retro-reflected signal. Nevertheless, this method implies that every parameter in Eq. 2 must be calibrated which in turn increases the risk of errors. Also, the configuration of the detecting platform that includes a modified Schmidt-Cassegrain telescope and a gated camera would make Eq. 2 much more complex. Instead of calculating the total amount of power, we decide to calibrate the response of the gated camera to a corner cube for which we know the OCS value. We assume that the transmitted power and the solid-angle of the transmitted-beam have constant values. We consider the optical transmission of the transmitter and the receiver as constant values as well. The distance to the target (R) is determined by the laser rangefinder with a precision of ±1.0 meter. The only parameters that are changing from one experiment to another are the atmospheric transmissions τ_1 and τ_2. Those parameters can be expressed as [3]:

$$\tau_1 \cdot \tau_2 = \tau_A = \exp\left[\frac{-7.82}{V}\left(\frac{\lambda}{0.55}\right)^{-q}\left(\frac{R}{1000}\right)\right] \qquad (3)$$

where V is the visibility (km), R the range (m) and λ the wavelength (μm).

This equation is valid for horizontal path at sea level. For higher altitude, the transmission increase. The values of q depend on the visibility, the size and the distribution of the scattering particles. The influence of the visibility is discussed later in this paper.

Because a gated camera with an amplified gain was chosen in the platform, it is important to quantify the implication of the gain before analyzing retro-reflected image. Fig. 5 shows the variation of the retro-reflected image of a given retro-reflector at different gain settings.

Figure 5. Images of retro-reflection signal of a retro-reflector at various gain settings.

As seen in Fig. 5, the retro-reflection image is often characterized by a very bright spot comparing to the background. This characteristic generally involves saturated pixels in center of the image. Fig. 6 shows the intensity profile of a line and the presence of saturated pixels in the center of the retro-reflected signal.

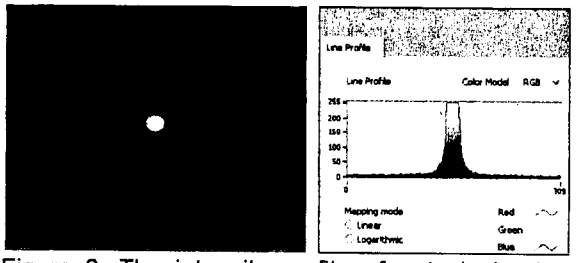

Figure 6. The intensity profile of a typical retro-reflected signal is characterized by saturated pixels. The green line in the left picture in the plan (x-y) is represented by the intensity profile of the image by the right picture (axis z).

The number of saturated pixels is used as a parameter measuring the amount of power of the retro-reflected beam. Each image of retro-reflection signal can be characterized by a formula that is a function of the gain (mV) of the gated camera, the distance (m) and then the number of saturated pixels.

5. THE EXPERIMENT

In the experimental setup, a corner cube is placed at different distances from the platform illustrated in

Fig. 3. A laser source is activated to illuminate the corner cube so that the synchronized gated camera detects a retro-reflected signal. As shown in Fig. 5, a series of image from a given retro-reflector are taken at different camera gain settings. Then, the OCS of the corner cube is varied by adding aperture masks and/or attenuating filters and images of retro-reflected signal are taken again in the same way. With three masks of different apertures (M1, M2 or M3) and two different attenuating filters (F1 or F2), it is possible to achieve nine OCS values. After this process, the whole experimental protocol is repeated at another distance. Results for a distance of 200 meters are presented at the Fig. 7.

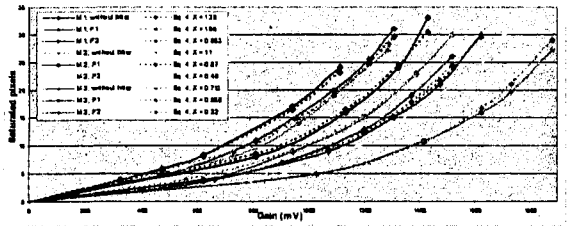

Figure 7. Number of saturated pixels from retro-reflection signals of a corner cube as a function of the camera gain for a distance of 200 meters.

In the graph presented in Fig. 7, curves drawn with continuous lines represent experimental values while curves in dash line are mathematical representations of experimental data. Curve with the same color are related. Dashed lines can be fitted with:

$$SP = (1.08^{G\cdot 0.0305} - 1 + 0.005\,G)\cdot \chi \qquad (4)$$

where SP is the number of saturated pixels, G is the gain (mV) and χ is a variable as a function of the OCS.

To connect Eq. 4 with values of OCS, we first attribute a normalized value of 1 to the mask with the largest aperture M1 and no filter. The values of the other OCS are obtained by a ratio in proportion to this value of 1. As shown in Fig. 7, a value of the χ factor can be related to a value of an OCS.

Fig. 8 shows the variation of the normalized OCS as a function of the χ parameter.

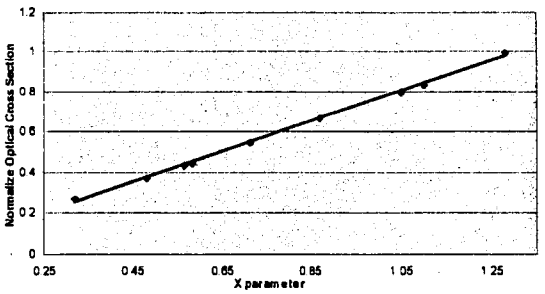

Figure 8. Variation of the normalized optical cross section as a function of the χ parameter

Fig. 8 demonstrates a linear relationship between the normalized OCS and χ that can be expressed by Eq. 5.

$$\sigma_{normalized} = 0.573\chi \qquad (5)$$

where 0.573 is the value of the slope (m).

Considering this graph and Eq. 4, the normalized OCS can be expressed as:

$$\sigma_{normalized} = \frac{SP\cdot m}{(1.08^{G\cdot 0.0305} - 1 + 0.005G)} \qquad (6)$$

where (m) is the slope of the graph of the OCS as a function of the χ parameter.

To extend Eq. 6 to other distances, one must find the relation between the slope (m) and the distance R.

To obtain this relation, another experiment has been done where the images of retro-reflected corner cubes obtained at different distances without changing the OCS were analyzed. Fig. 9 shows the variation of the χ parameter in function of the distance.

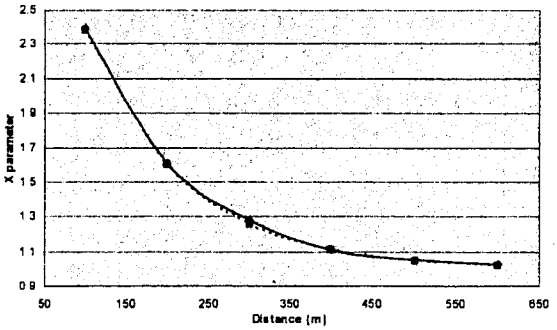

Figure 9. Variation of the χ parameter as a function of the distance for a corner cube without varying the OCS.

As in Fig. 7, a dash line curve is superposed to the experimental data and fitted with:

$$\chi = (0.78^{\frac{R(m)}{30}}) \cdot 3.2 + 1 \quad (7)$$

where R is the distance in meter.

By substituting Eq. 7 into Eq. 6, a final equation can be obtained.

$$\sigma^{*}_{normalized} = \frac{SP}{(1.08^{G \cdot 0.0305} - 1 + 0.005G)\left[(0.78^{\frac{R(m)}{30}}) \cdot 3.2 + 1\right]} \quad (8)$$

*(λ = 859 nm)

Eq. 8 represents the calculation of a normalized OCS as a function of the number of saturated pixels, the gain of the camera and the distance to the target. This formula is related to the platform shown in Fig. 3 and is also related to the properties of the laser source used for interrogation.

An experiment was done to validate the approach with a laser source operating at 859 nm and another operating at 532 nm. These wavelengths are situated in the centre of the visible spectrum where focalization has better chance to be optimal and at a longer wavelength where it can be detected by the phosphor plate of the gated camera. Sources in ultra-violet region are not taken because some materials which lenses are made do not allow good optical transmission.

After repeating the same experimental protocol explained above, a formula of the normalized OCS for the laser source at 532 nm can be calculated:

$$\sigma^{*}_{normalized} = \frac{SP}{(1.08^{G \cdot 0.0305} - 1 + 0.005G)\left[(0.65^{\frac{R(m)}{32}}) \cdot 59 + 0.09\right]} \quad (9)$$

*(λ = 532 nm)

Fig. 10 a) shows typical OSs mixed with false alarms sources. Those objects were illuminated at the two selected wavelengths, 859 nm in Fig.10 b) and 532 nm in Fig.10 c). The red circle shows retro-reflected images of a binocular with a calculated normalized OCS of 0.51 at 532 nm and 0.33 at 859 nm. Fig.10 b) and Fig.10 c) illustrate in the green circle the absence of retro-reflected signal at 532 nm for a red retro-reflector while it is highly visible with the infrared source. Therefore, this retro-reflector acts as a low band filter. This false alarm is useful to be eliminated as its presence in urban environment is very important. Finally, as shown in Fig. 10, it is possible to perform multiple simultaneous analyzes as each signal can be processed independently. This is an important issue as the platform should be operating in urban area where a lot of clutter can occur.

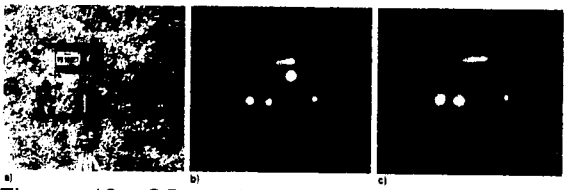

Figure 10. OS and typical false alarms are illustrated in a). The images of b) and c) show the retro-reflection signals at a wavelength of 859 and 532 nm respectively.

6. LIMITATIONS

The method shows encouraging results, however it has limitations. The visibility can involve errors on the measure that can affect the % of transmission in atmosphere. Therefore, before taking measurements, it is important to calibrate the platform. To achieve the calibration, a corner cube whose OCS is known can provide the value of the visibility in the operating condition. By doing a calibration before each operation, the platform can theoretically be used in every atmospheric condition.

Other errors on the experimental measures were not considered in this paper and will need to be quantified in future works as we will evaluate the efficiency of the method. First, errors can be caused by atmospheric turbulence by degrading the quality of the images. The effect of atmospheric turbulence will have to be quantified as it can change depending on the weather and the distance. Also, Eqs. 8 and 9 were obtained by taking the shape of a retro-reflected signal from a corner cube. Some studies [5][6] have shown that the shape of retro-reflected signal can be slightly different in function of the retro-reflector. An evaluation of this impact on results has to be done yet. Another error can be created by the uniformity in power of the emissive source as well as the steadiness of the power in time. Moreover, vigneting effect [2][7] may influence the value of the OCS if the OSs are not facing the detecting platform. Finally, for very small OCSs, the gain of the gated camera needs to be high, causing more noise. However, it is possible to diminish the effect of the noise by taking image of the background of the scene without laser illumination and then subtracting it to the retro-reflected signal.

7. CONCLUSION

We presented a method for the identification and the recognition of OSs. Eq. 8 and 9 are considered as qualitative as they are valid only for the imaging platform described and the proprieties of the laser sources that were used. Results show a promising method to identify OSs by getting value of OCS from image of retro-reflected signals at different wavelengths. Nevertheless, a lot of works has to

be done to improve the performance and the efficiency of the method. First, more measurements must be done to validate the hypothesis done. Then, it will be important to quantify the error made in each value of OCS calculated. Finally, the system needs to be tested in real environment to evaluate the rate of recognition of OSs.

REFERENCES

1. R.O. Wilson, Nashua N.H. (1995). Apparatus and method for highlighting returns from optically augmented targets. *United States Patent.* Number 5449899.
2. Norman R. Wild, Paul M. Leavy Jr. (2003). Optical Detection System. *United States Patent*, Number 6603134 B1.
3. Svalgaard, W. L. Wolfe, G.J Zissis. (1989). The Infrared Handbook. *Office of Naval Research, Departement of the Navy*, (1989), 23-6.
4. S B.E.A Saleh and M.C. Teich. (1991). Fundamentals of photonics. *John Wiley & sons.* pp.644-695.
5. Dmitry Kiesewetter. (2004). Numerical simulation of the retroreflection by glass beads. *SPIE* Vol 5400 pp.185-188.
6. S.K. Nayar, K. Ikeuchi, T. Kanade. (1989). Determine Shape and Reflectance of Lambertian, Specular and Hybrid Surfaces using Extended Sources. *IEEE.*
7. W.S. Rabinovich, R. Mahon, P. Goetz, E. Waluschka, D.S. Katzer, S.Binari and G. C. Gilbreath. (2003). A Cat's Eye Multiple Quantum Well Modulating Retro-reflector. *SPIE Vol 4975.*

REMOTE IDENTIFICATION OF OPTICAL SYSTEMS BY TIME-GATED MULTI-WAVELENGTH RETRO-REFLECTION

Michel Auclair [1], Jean Fortin [2], Yunlong Sheng [1]

[1] *Center for Optics, Photonics and Lasers, Laval University, Québec, Canada, G1K 7P4, Michel.Auclair.UN-LAVAL@drdc-rddc.gc.ca, sheng@phy.ulaval*
[2] *Defence R&D Canada - Valcartier, 2459 Boul. Pie XI N, Québec, Canada G3J 1X5, Jean.Fortin@drdc-rddc.gc.ca*

ABSTRACT

We propose and demonstrate a multi-wavelength approach based on time-gated retro-reflection to discriminate false alarms from optical systems (OSs). Any objects other than optical systems are considered as false alarms. The detecting platform consists in a combination of a pulsed laser synchronized with a gated camera and a laser rangefinder. A Schmidt-Cassegrain telescope was modified to inject the light of laser sources and to collect the retro-reflected signal in a monostatic configuration.

The filtering method is based on the chromatic aberrations of the optical systems of interest which are measured using multiple interrogation wavelengths. A formula to evaluate the optical cross section (OCS) at the selected wavelengths is used for identification and relies on the system signature to discriminate the false alarms. We also explore the possibility to perform multiple simultaneous detections and target identification.

1. INTRODUCTION

Detection of optical systems is a real challenge as they are difficult to recognize in a complex background. Some studies have already shown the possibility to detect optical systems by using the technique of retro-reflection [1][2]. However, a robust solution has not yet been found to solve the problem of recognizing optical systems by retro-reflection in urban environment. In fact, retro-reflected signals of OS are often confused with spurious detections of many other objects that can reflect light.

In this article, an approach to discriminate false alarms from OS using a time-gated retro-reflection is first proposed. Then, the design of a platform for detection is presented and finally an experiment shows results that make possible to identify OS and discriminate false alarms.

2. APPROACH FOR IDENTIFICATION OF OPTICAL SYSTEMS

The term OS in this paper represents "any optical instrument which includes a focusing lens and a surface having some degree of reflectivity, no matter how small, positioned near the focal point of the lens" [2]. A retro-reflector is defined as "a reflector wherein incident rays or radiant energy and reflected rays are parallel for any angle of incidence within the field of view" [2]. An OS can act as a retro-reflector.

To be able to identify different OSs, it is necessary to associate them to their signature. As we are detecting radiation from retro-reflection, the signature must be calculated from the measured OCS.

In retro-reflection, the OCS [3] can be expressed as:

$$\sigma = \frac{\rho A}{\Omega} \qquad (1)$$

where ρ is the reflectivity, A the area of the target and Ω the solid angle of the return beam. By this definition, each OS has a different OCS. However, two systems can have very close OCS values and as it is calculated from detected radiation, it is possible to wrongly associate a value of OCS to objects that reflect light with a similar way than the retro-reflected signals of a target OS, hence causing false-alarms. One way to solve this problem is to use multiple laser sources with different wavelengths and measure the variation of the OCS as a function of the wavelength. As it is shown in the Fig. 1, the focalization point of rays, made by a set of lens inside an OS, may slightly be different depending on the wavelength of illumination. This phenomenon is caused by the variation of the refractive index of the lenses with the wavelength and also because the optical design is not always perfectly achromatic. To have a significant difference on the focalization point, it is important to use wavelengths with distant values, such as one in the visible and another one

in the near infrared. In fact, OS that are designed to be used in the visible are generally not achromatic in the near infrared region.

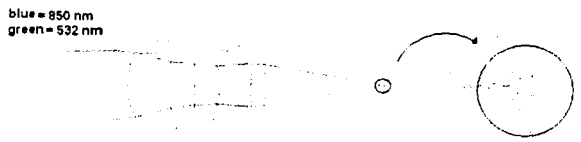

Figure 1. Illustration of the quality of focalization when using two different wavelengths (850 nm shown in blue and 532 nm in green) in a typical camera objective.

Optical simulations have been made on typical OSs to look at the impact of the wavelength on the focalization point. As shown in Fig. 2, the solid angle of the retro-reflected beam changes as a function of the illumination wavelength and at some distance the difference on the diameter is significant.

Figure 2. Illustration of the diameter of a retro-reflected beam at 500 meters for an illumination sources at 532 nm (in green) and 850 nm (in blue).

Because all OSs have their own design, the variation between the OCS taken at different wavelengths is unique. This is useful to eliminate false alarms.

False alarms are defined as any objects other than OSs. For them, the variation in the OCS measured as a function of the wavelength is not in the same order. For example, a white retro-reflector installed on a car (or bicycle) has in theory an OCS independent of the wavelength because it is made of many small reflective mirror cavities that reflect light regardless of wavelength. The same phenomenon occurs for specular reflections on reflective materials.

3. DETECTION PLATFORM

The detection platform consists in a combination of a pulsed laser synchronized with a gated camera and a laser rangefinder. A Schmidt-Cassegrain telescope was modified to inject the light of laser sources and collect the retro-reflected signal in a monostatic configuration. Fig. 3 illustrates a preliminary version of a laboratory prototype.

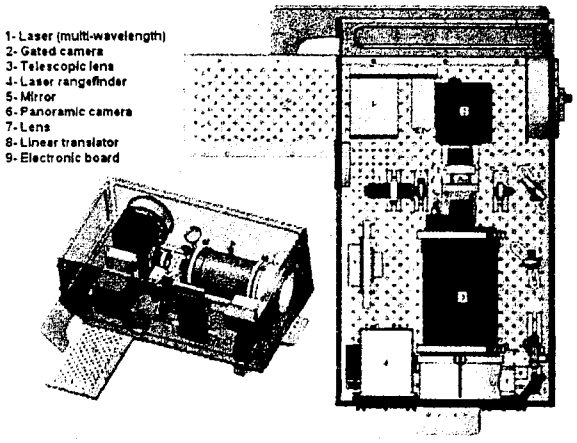

Figure 3. Platform designed for detecting retro-reflected signals.

The laser rangefinder gives the distance of objects in the area of interrogation. Then, a time-gated camera in synchronization with the pulsed laser produces a high contrast image of the signal retro-reflected by a potential target OS. The signal to noise ratio is increased by using interferential filters in front of the gated camera and centered on the wavelength of the laser source. Finally, the focus for getting the well-defined image at different distances is made by a translation of the gated-camera on a linear translator. The narrow field of view of the gated camera is centered in the field of view of a panoramic camera operating in the visible spectrum. This sensor gives a contextual view of the scene and helps the operator searching for areas of interest. Fig. 4 shows an image of the platform user interface. The top part shows an image produced by a panoramic camera. The bottom part shows the high contrast image of a 15 mm diameter retro-reflector at 600 meters in bright daylight.

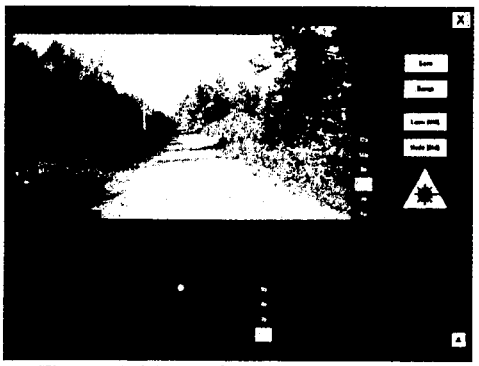

Figure 4. View of the user interface.

The gated camera contains an imaging photocathode which converts photons to electrons. The photoelectrons are then accelerated by an electric field and multiplied by a micro channel plate. It consists of an array of millions capillaries

in a thin glass plate. Both faces of the plate are coated with thin metal films that act as electrodes and a voltage is applied across them. The interior walls of each capillary are coated with a secondary-electron-emissive material and behave as a continuous dynode, multiplying the photoelectron current emitted at that position. The local photon flux in an image can be rapidly converted into a substantial electron flux [4]. The highly intensified electron flux strikes a phosphor screen and provides electroluminescence that created an amplified image. Finally the image can be seen with a Silicon CCD camera which has horizontally 639 effective pixels and vertically 479 effective pixels. Each pixel has a dimension of 9.9μm x 9.9μm. The sensitivity of the photocathode is approximately 65 mA/W at a wavelength of 532 nm and 50 mA/W at 859 nm. The gain for amplification can be adjusted from 0 to 2500 mV.

4. THEORY OF THE EXPERIMENT

The purpose of the experimentation is to get data that will lead to a relation between retro-reflected signals and the OCS. The relation should be expressed by a mathematical formula. We first consider the theoretical relation between detected power in retro-reflection and the OCS [3]:

$$\Phi_R = \frac{\pi \Phi_T D^2}{4 \Omega_T R^4} \tau_1 \tau_2 \tau_T \tau_r \sigma \qquad (2)$$

where Φ_T is the transmitted power (W), Ω_T the transmitted-beam solid-angle (sr), τ_1 and τ_2 the one way path transmission, R the one-way range (m), D the receiver diameter (m), τ_T the transmitter optical transmission, τ_r the receiver optical transmission and σ the OCS of the target (m^2/sr).

Consequently, one method to calculate the value of OCS is to measure the amount of retro-reflected signal. Nevertheless, this method implies that every parameter in Eq. 2 must be calibrated which in turn increases the risk of errors. Also, the configuration of the detecting platform that includes a modified Schmidt-Cassegrain telescope and a gated camera would make Eq. 2 much more complex. Instead of calculating the total amount of power, we decide to calibrate the response of the gated camera to a corner cube for which we know the OCS value. We assume that the transmitted power and the solid-angle of the transmitted-beam have constant values. We consider the optical transmission of the transmitter and the receiver as constant values as well. The distance to the target (R) is determined by the laser rangefinder with a precision of ±1.0 meter. The only parameters that are changing from one experiment to another are the atmospheric transmissions τ_1 and τ_2 and those parameters can be expressed as [3]:

$$\tau_1 \cdot \tau_2 = \tau_A = \exp\left[\frac{-7.82}{V}\left(\frac{\lambda}{0.55}\right)^{-q}\left(\frac{R}{1000}\right)\right] \qquad (3)$$

where V is the visibility (km), R the range (m) and λ the wavelength (μm).

This equation is valid for horizontal path at sea level. For higher altitude, the transmission increases. The values of q depend on the visibility, the size and the distribution of the scattering particles. The influence of the visibility is discussed later in this paper.

Because a gated camera with an amplified gain was chosen in the platform, it is important to quantify the implication of the gain before analyzing retro-reflected image. Fig. 5 shows the variation of the retro-reflected image of a given retro-reflector at different gain settings.

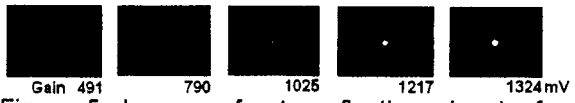

Figure 5. Images of retro-reflection signal of a retro-reflector at various gain settings.

As seen in Fig. 5, the retro-reflection image is often characterized by a very bright spot comparing to the background. This characteristic generally involves saturated pixels in center of the image. Fig. 6 shows the intensity profile of a line and the presence of saturated pixels in the center of the retro-reflected signal.

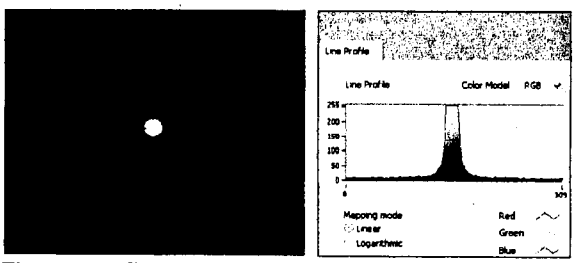

Figure 6. The intensity profile of a typical retro-reflected signal is characterized by saturated pixels. The green line in the left picture in the plan (x-y) is represented by the intensity profile of the image by the right picture (z axis).

The number of saturated pixels is used as a parameter measuring the amount of power of the retro-reflected beam. Each image of retro-reflection signal can be characterized by a formula that is a function of the gain (mV) of the gated camera, the distance (m) and then the number of saturated pixels.

5. THE EXPERIMENT

In the experimental setup, a corner cube is placed at different distances from the platform illustrated in

Fig. 3. A laser source is activated to illuminate the corner cube so that the synchronized gated camera detects a retro-reflected signal. As shown in Fig. 5, a series of image from a given retro-reflector are taken at different camera gain settings. Then, the OCS of the corner cube is varied by adding aperture masks and/or attenuating filters and images of retro-reflected signal are taken again in the same way. With three masks of different apertures (M1, M2 or M3) and two different attenuating filters (F1 or F2), it is possible to achieve nine OCS values. After this process, the whole experimental protocol is repeated at another distance. Results for a distance of 200 meters are presented at the Fig. 7.

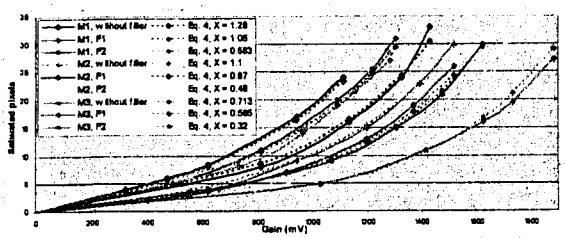

Figure 7. Number of saturated pixels from retro-reflection signals of a corner cube as a function of the camera gain for a distance of 200 meters.

In the graph presented in Fig. 7, curves drawn with continuous lines represent experimental values while curves in dash line are mathematical representations of experimental data. Curve with the same color are related. Dashed curves can be fitted with:

$$SP = (1.08^{G\cdot 0.0305} - 1 + 0.005\,G)\cdot \chi \qquad (4)$$

where SP is the number of saturated pixels, G is the gain (mV) and χ is a variable as a function of the OCS.

To connect Eq. 4 with values of OCS, we first attribute a normalized value of 1 to the mask with the largest aperture M1 and no filter. The values of the other OCS are obtained by a ratio in proportion to this value of 1. As shown in Fig. 7, a value of the χ factor can be related to a value of an OCS.

Fig. 8 shows the variation of the normalized OCS as a function of the χ parameter.

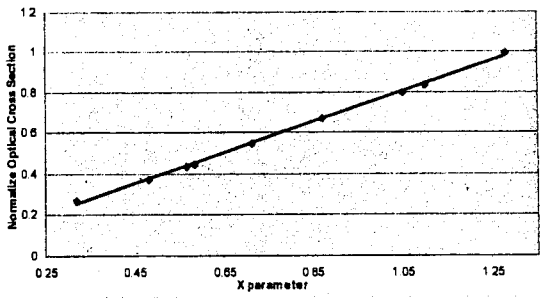

Figure 8. Variation of the normalized optical cross section as a function of the χ parameter

Fig. 8 demonstrates a linear relationship between the normalized OCS and χ that can be expressed by Eq. 5.

$$\sigma_{normalized} = 0.573\chi \qquad (5)$$

where 0.573 is the value of the slope (m).

Considering this graph and Eq. 4, the normalized OCS can be expressed as:

$$\sigma_{normalized} = \frac{SP\cdot m}{(1.08^{G\cdot 0.0305} - 1 + 0.005G)} \qquad (6)$$

where (m) is the slope of the graph of the OCS as a function of the χ parameter.

To extend Eq. 6 to other distances, one must find the relation between the slope (m) and the distance R.

To obtain this relationship, another experiment has been done where the images of retro-reflected corner cubes obtained at different distances without changing the OCS were analyzed. Fig. 9 shows the variation of the χ parameter as a function of the distance.

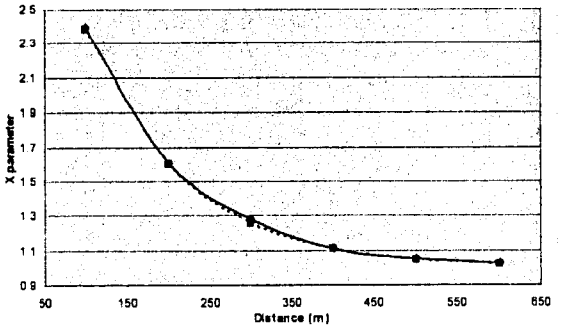

Figure 9. Variation of the χ parameter as a function of the distance for a corner cube without varying the OCS.

As in Fig. 7, a dashed curve is superposed to the experimental data and fitted with the following expression:

$$\chi = (0.78^{\frac{R(m)}{30}}) \cdot 3.2 + 1 \quad (7)$$

where R is the distance in meter.

By substituting Eq. 7 in Eq. 6, one obtains:

$$\sigma^{\circ}_{normalized} = \frac{SP}{(1.08^{G \cdot 0.0305} - 1 + 0.005G)\left[(0.78^{\frac{R(m)}{30}}) \cdot 3.2 + 1\right]} \quad (8)$$

*(λ = 859 nm)

Eq. 8 represents normalized OCS values as a function of the number of saturated pixels, the gain of the camera and the distance to the target. This formula is valid for the platform described in Fig. 3 and is also related to the properties of the laser source used for interrogation.

An experiment was done to validate the approach with a laser source operating at 859 nm and another one operating at 532 nm. These wavelengths are situated in the centre of the visible spectrum where focalization has better chance to be optimal and at a longer wavelength where it can be detected by the phosphor plate of the gated camera. Sources in ultra-violet region are not taken because some materials which lenses are made do not allow good optical transmission.

After repeating the experimental protocol explained above, a formula of the normalized OCS for the laser source at 532 nm can be calculated:

$$\sigma^{\circ}_{normalized} = \frac{SP}{(1.08^{G \cdot 0.0305} - 1 + 0.005G)\left[(0.65^{\frac{R(m)}{32}}) \cdot 59 + 0.09\right]} \quad (9)$$

*(λ = 532 nm)

Fig. 10 a) shows the images of typical OSs mixed with false alarms sources. Those objects were illuminated at the two selected wavelengths, 859 nm in Fig.10 b) and 532 nm in Fig.10 c). The red circle shows the retro-reflected images of a binocular with a calculated normalized OCS of 0.51 at 532 nm and 0.33 at 859 nm. Fig.10 b) and Fig.10 c) illustrate in the green circle the absence of retro-reflected signal at 532 nm for a red retro-reflector while it is highly visible with the near infrared source. Therefore, this retro-reflector acts as a low band filter. This false alarm is useful to be eliminated as its presence in urban environment is very important. Finally, as shown in Fig. 10, it is possible to perform multiple simultaneous analyzes as each signal can be processed independently. This is an important issue as the platform should be operating in urban area where a lot of clutter can occur.

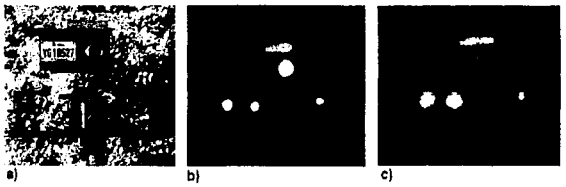

Figure 10. OS and typical false alarms are illustrated in a). The images of b) and c) show the retro-reflection signals at a wavelength of 859 and 532 nm respectively.

6. LIMITATIONS

The method shows encouraging results, however it has limitations. The visibility can involve errors on the measurements that can affect the % of transmission in the atmosphere. Therefore, before taking measurements, it is important to calibrate the platform. To achieve the calibration, a corner cube whose OCS is known can provide the value of the visibility in the operating condition. By doing a calibration before each operation, the platform can theoretically be used in every atmospheric condition.

Other errors on the experimental measures were not considered in this paper and will need to be addressed in future works as we will evaluate the efficiency of the method. First, errors can be caused by atmospheric turbulence by degrading the quality of the images. The effect of atmospheric turbulence will have to be quantified as it can change depending on the weather and the distance. Also, Eqs. 8 and 9 were obtained by taking the shape of a retro-reflected signal from a corner cube. Some studies [5][6] have shown that the shape of retro-reflected signal can be slightly different depending on the retro-reflector. An evaluation of this impact on results has to not been done yet. Another error can be created by the uniformity in power of the emissive source as well as the steadiness of the power in time. Moreover, vigneting [2][7] may influence the value of the OCS if the OSs are not facing the detection platform. Finally, for very small OCSs, the gain of the gated camera needs to be high, causing more noise. However, it is possible to diminish the effect of the noise by taking image of the background of the scene without laser illumination and then subtracting it to the retro-reflected signal.

7. CONCLUSION

We presented a method for the identification and the recognition of OSs. Eq. 8 and 9 are considered as qualitative as they are valid only for the imaging platform described and the properties of the laser sources that were used. Results show a promising method to identify OSs by getting value of OCS from image of retro-reflected signals at different wavelengths. Nevertheless, a lot of works has to

be done to improve the performance and the efficiency of the method. First, more measurements must be done to validate the main hypothesis. Then, it will be important to quantify the error made in each value of OCS calculated. Finally, the system needs to be tested in real environment to evaluate the rate of recognition of OSs.

REFERENCES

1. R.O. Wilson, Nashua N.H. (1995). Apparatus and method for highlighting returns from optically augmented targets. *United States Patent.* Number 5449899.
2. Norman R. Wild, Paul M. Leavy Jr. (2003). Optical Detection System. *United States Patent*, Number 6603134 B1.
3. Svalgaard, W. L. Wolfe, G.J Zissis. (1989). The Infrared Handbook. *Office of Naval Research, Departement of the Navy*, (1989), 23-6.
4. S B.E.A Saleh and M.C. Teich. (1991). Fundamentals of photonics. *John Wiley & sons.* pp.644-695.
5. Dmitry Kiesewetter. (2004). Numerical simulation of the retroreflection by glass beads. *SPIE* Vol 5400 pp.185-188.
6. S.K. Nayar, K. Ikeuchi, T. Kanade. (1989). Determine Shape and Reflectance of Lambertian, Specular and Hybrid Surfaces using Extended Sources. *IEEE.*
7. W.S. Rabinovich, R. Mahon, P. Goetz, E. Waluschka, D.S. Katzer, S:Binari and G. C. Gilbreath. (2003). A Cat's Eye Multiple Quantum Well Modulating Retro-reflector. *SPIE Vol 4975.*